Vibrational Responses of Bound and Nonbound Targeted Lipid-Coated Single Microbubbles

Tom van Rooij, *Member, IEEE*, Inés Beekers, *Student Member, IEEE*, Kirby R. Lattwein, Antonius F. W. van der Steen, *Fellow, IEEE*, Nico de Jong, *Member, IEEE*, and Klazina Kooiman, *Member, IEEE*

***Abstract*— One of the main challenges for ultrasound molecular imaging is acoustically distinguishing nonbound microbubbles from those bound to their molecular target. In this *in vitro* study, we compared two types of in-house produced targeted lipid-coated microbubbles, either consisting of 1,2-dipalmitoyl-*sn*-glycero-3-phosphocholine, C16:0 (DPPC) or 1,2-distearoyl-*sn*-glycero-3-phosphocholine, C18:0 (DSPC) as the main lipid, using the Brandaris 128 ultrahigh-speed camera to determine vibrational response differences between bound and nonbound biotinylated microbubbles. In contrast to previous studies that studied vibrational differences upon binding, we used a covalently bound model biomarker (i.e., streptavidin) rather than physisorption, to ensure binding of the biomarker to the membrane. The microbubbles were insonified at frequencies between 1 and 4 MHz at pressures of 50 and 150 kPa. This paper shows lower acoustic stability of bound microbubbles, of which DPPC-based microbubbles deflated most. For DPPC microbubbles with diameters between 2 and 4 μm driven at 50 kPa, resonance frequencies of bound microbubbles were all higher than 1.8 MHz, whereas those of nonbound microbubbles were significantly lower. In addition, the relative radial excursions at resonance were also higher for bound DPPC microbubbles. These differences did not persist when the pressure was increased to 150 kPa, except for the acoustic stability which further decreased. No differences in resonance frequencies were observed between bound and nonbound DSPC microbubbles. Nonlinear responses in terms of emissions at the subharmonic and second harmonic frequencies were similar for bound and nonbound microbubbles at both pressures. In conclusion, we identified differences in vibrational responses of bound DPPC microbubbles with diameters between 2 and 4 μm that distinguish them from nonbound ones.**

***Index Terms*— Biotin-streptavidin, lipid-coating, molecular imaging, nonlinear behavior, targeted microbubbles, ultrahigh-speed optical imaging, ultrasound contrast agents.**

Manuscript received November 3, 2016; accepted March 3, 2017. Date of publication March 7, 2017; date of current version May 1, 2017. This work was supported in part by NanoNextNL, a microtechnology and nanotechnology consortium of the Government of The Netherlands, in part by the Center for Translational Molecular Medicine, and in part by the Netherlands Heart Foundation (PARISk).

T. van Rooij, I. Beekers, K. R. Lattwein, and K. Kooiman are with the Department of Biomedical Engineering, Thorax Center, Erasmus MC, 3000 Rotterdam, The Netherlands (e-mail: tvrooij@gmail.com).

A. F. W. van der Steen and N. de Jong are with the Department of Biomedical Engineering, Thorax Center, Erasmus MC, 3000 Rotterdam, The Netherlands, and also with the Laboratory of Acoustical Wavefield Imaging, Faculty of Applied Sciences, Delft University of Technology, 2628 Delft, The Netherlands and also with the Netherlands Heart Institute, 3511 Utrecht, The Netherlands.

This paper has supplementary downloadable material available at http://ieeexplore.ieee.org., provided by the author. Ultrahigh-speed recordings of a bound DPPC and DSPC microbubble insonified at a pressure of 50 and 150 kPa and a frequency of 1 and 4 MHz.

Digital Object Identifier 10.1109/TUFFC.2017.2679160

I. Introduction

ULTRASOUND contrast agents that consist of targeted microbubbles are emerging in their applications for ultrasound molecular imaging [1]–[3]. These microbubbles have a ligand attached to their shell by which they can be targeted to a specific biomarker, for example, $\alpha_v\beta_3$ that is expressed on the cellular membrane of endothelial cells in neovasculature [4], [5]. For successful translation of ultrasound molecular imaging to the clinic, two major problems still need to be tackled: 1) producing microbubbles of the same size that also behave identical in an ultrasound field and 2) distinguishing the response of a single targeted microbubble bound to a specific biomarker from a nonbound targeted microbubble. Since microbubbles of the same size can still have different acoustic properties [6]–[10], producing monodisperse microbubbles may not necessarily result in microbubbles that have, for example, the same resonance frequency. But if it is possible to determine the acoustic parameters that are specific for bound targeted microbubbles, they may be distinguished from nonbound targeted microbubbles based on their acoustic signal. Several studies investigated the difference in acoustic properties of bound and nonbound microbubbles, but these studies reported conflicting results. In the low-frequency range (2–4 MHz) a shift in resonance frequency was found for microbubbles after binding [11], [12], whereas at 11 and 25 MHz no shift was observed [13]. For the responses at the subharmonic frequency either a change in frequency [13] or no change in amplitude and frequency [14] was reported upon binding. In contrast, for the response at the second harmonic frequency, the results reported in [14] and [15] were in agreement with each other: the amplitude increased for bound microbubbles. Finally, Overvelde *et al.* [12] and Zhao *et al.* [14] found a decrease in the vibrational response at the fundamental frequency for bound microbubbles.

All acoustic studies on bound versus nonbound targeted microbubbles used either physisorption as a method to attach a model biomarker to an artificial surface (membrane or capillary) [11], [12], [14], [15] or had the model biomarker embedded in agarose [13]. Physisorption or physical adsorption relies on electrostatic binding through van der Waals forces between the biomarker and the membrane, but is in fact a very weak bond [16], which can result in detachment of the biomarker from the membrane or capillary. As a result, the biomarker can cover the whole targeted microbubble, including the area that is not directly in contact with the membrane. This was

reported in [17] for the model biomarker streptavidin that was physisorbed to an OptiCell membrane. Functionalization of lipid-coated microbubbles with streptavidin changes the properties, such as elasticity [18]–[20] and acoustic stability [20]. Consequently, the comparisons made in previous studies between bound microbubbles and nonbound microbubbles are in fact a comparison between bound lipid-coated microbubbles covered by streptavidin and nonbound lipid-coated microbubbles, which did not have streptavidin on their shell. In addition, both physisorption and embedding a model biomarker in agarose are far from the *in vivo* situation, where biomarkers are incorporated into the cellular membrane.

We covalently linked a model biomarker to an artificial surface to study the vibrational responses of single bound targeted microbubbles and nonbound targeted microbubbles aiming to find parameters to discriminate them acoustically. Super-resolution confocal laser scanning fluorescence microscopy showed that covalent coupling of the model biomarker streptavidin to a hydrogel prevented the streptavidin to bind to the biotinylated lipid-shell of the microbubble outside the binding area [21]. That study compared the lipid distribution and binding area of two types of targeted lipid-coated microbubbles that were either coated with mainly 1,2-dipalmitoyl-*sn*-glycero-3-phosphocholine, C16:0 (DPPC) which is the main shell component of Definity (Lantheus Medical Imaging, North Billerica, MA, USA) or mainly 1,2-distearoyl-*sn*-glycero-3-phosphocholine, C18:0 (DSPC) which is the main lipid component of SonoVue, Lumason, and BR14 (Bracco Imaging S.p.A., Milan, Italy) [10], [21]–[25]. It was shown that the lipid distribution was more homogeneous for DPPC-based microbubbles than for DSPC-based microbubbles and that the binding area for DPPC-based microbubbles was significantly larger than for DSPC-based microbubbles [21]. We previously determined the acoustic properties of these DPPC and DSPC-based microbubbles in a setup where the microbubbles were floating against an OptiCell wall (nonbound) [10] and hypothesized that the difference in ligand distribution and binding area could alter the acoustic response after adherence of the microbubble to its molecular target. In this paper, we investigated the vibrational response of in-house produced targeted DPPC-based and DSPC-based microbubbles using the Brandaris 128 ultrahigh-speed optical camera [26] when they had bound to a streptavidin-coated hydrogel and compared their responses to those of nonbound microbubbles floating against the hydrogel. We aimed to identify differences in vibrational responses that may be used to discriminate bound from nonbound microbubbles.

II. Materials and Methods

A. Microbubble Preparation

Biotinylated lipid-coated microbubbles with a C_4F_{10} gas core (F2 Chemicals Ltd, Preston, UK) were made as previously described [21], [27] by sonication for 1 min. The coating was composed of 59.4 mol% DSPC (P6517, Sigma-Aldrich, Zwijndrecht, The Netherlands) or DPPC (850355, Avanti Polar Lipids, Alabaster, AL, USA), 35.7 mol% polyoxyethylene-40-stearate (PEG-40 stearate, P3440, Sigma-Aldrich), 4.1 mol% 1,2-distearoyl-*sn*-glycero-3-phosphoethanolamine-N-[carboxy(polyethylene glycol)-2000] (DSPE-PEG(2000), 880125, Avanti Polar Lipids); and 0.8 mol% 1,2-distearoyl-*sn*-glycero-3-phosphoethanolamine-N-[biotinyl(polyethylene glycol)-2000] [DSPE-PEG(2000)-biotin, 880129, Avanti Polar Lipids].

A 25-μm-thick polyester membrane was mounted on a custom-made rectangular polyvinylchloride holder (same size as a microscope objective glass) and was custom-coated with a 1–2-μm-thick polycarboxylate hydrogel (XanTec bioanalytics GmbH, Düsseldorf, Germany). For the bound targeted microbubbles, the hydrogel was activated and streptavidin (S4762, Sigma-Aldrich) was subsequently covalently attached to the hydrogel, using the amine coupling kit (K AN-50, XanTec bioanalytics GmbH) according to the instructions of the manufacturer, as previously described [21]. Briefly, streptavidin was dissolved in acetate buffer (2 mM, pH 5.4) (1 mg/mL). After desalting the streptavidin by use of a PD-10 desalting column (GE Healthcare Bio-Sciences), the concentration was determined spectrophotometrically at 570 nm using a Pierce BCA Protein Assay kit (Thermo Scientific) and Thermo Multiskan EX. Three polyester membranes were placed in a 5-Slidemailer (Heathrow Scientific, Northgate, U.K.) with 18 mL of 1 M NaCl + 0.1 M NaB (pH 10) elution buffer (K AN-50, XanTec bioanalytics GmbH), followed by an incubation with 18 mL of 1.6% (w/v) EDC · HCL (K AN-50, XanTec bioanalytics GmbH) in activation NHS/MES buffer (K AN-50, XanTec bioanalytics GmbH), and 18 mL of 33 μg/mL desalted streptavidin in 2 mM acetate buffer at pH 5.2–5.4. Finally, 18 mL of 1 M ethanolamine hydrochloride (pH 8.5) quenching buffer (K AN-50, XanTec bioanalytics GmbH) was used to terminate the reaction. The targeted microbubbles were allowed to adhere to the streptavidin-coated membrane in air-equilibrated phosphate buffered saline (PBS) containing calcium and magnesium (DPBS, 14080, Invitrogen, Thermo Fischer Scientific, Landsmeer, The Netherlands) by flotation for 5 min. Then, the membrane was gently washed three times with air-equilibrated PBS containing calcium and magnesium using a 3 mL plastic Pasteur pipette. For the nonbound targeted microbubbles the hydrogel was treated in the same way, except for the addition of streptavidin. The targeted microbubbles were added below the hydrogel-coated polyester membrane of the custom-made holder and floated up due to buoyancy. The hydrogels with the nonbound targeted microbubbles and bound targeted microbubbles were orientated in the setup as shown in Fig. 1.

B. Microbubble Spectroscopy

The vibrational responses of the bound and nonbound targeted microbubbles were captured using the Brandaris 128 ultrahigh-speed camera operated at ~15 million frames/s [26]. Single microbubbles were investigated in Region Of Interest (ROI) mode [28] using the microbubble spectroscopy technique [6] in combination with the exact same setup as in [10], except for a higher magnification microscope objective (60×, NA = 0.9,

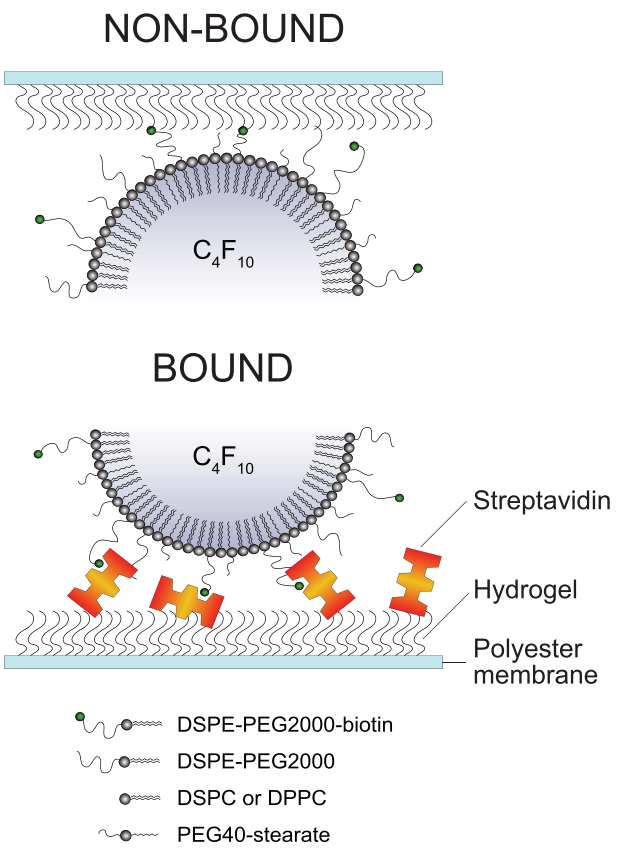

Fig. 1. Configuration and composition of nonbound targeted microbubbles (top) floating against a hydrogel and targeted microbubbles bound to this hydrogel via streptavidin (bottom) in the experimental setup (not to scale).

Olympus, Tokyo, Japan). Briefly, a broadband single element polyvinyl difluoride (PVDF) transducer (25-mm focal distance, f-number 1.1, center frequency 5 MHz, PA275, Precision Acoustics Ltd, Dorchester, UK) transmitted a Gaussian tapered eight-cycle sine wave burst at transmit frequencies swept from 1 to 4 MHz (increment steps of 200 kHz) at a peak-negative pressure (P_A) of 50 or 150 kPa at the focus. The pressures were calibrated with two calibrated PVDF needle hydrophones in a separate measurement beforehand (0.2-mm diameter PA2030 and 1-mm diameter PA1875, Precision Acoustics). The optic focus was aligned with the acoustic focus, to ensure that the microbubble received the intended pressure. The ultrasound was triggered on the second recording of each microbubble to obtain the initial resting diameter and the noise level with our contour tracking algorithm in the first recording. The experiments were conducted at room temperature and the sample was submersed in air-equilibrated PBS containing calcium and magnesium. All microbubbles were exposed to ultrasound within 2 h after addition to the custom-made holder.

C. Data Analysis

Diameter-time (*D-t*) curves were obtained using custom-designed image analysis software [6] that determines the vibrational responses as described elsewhere [10]. Briefly, the acoustic stability of the microbubbles was quantified as the difference between the mean diameter of the microbubble in the initial *D-t* curve (D_0) and the final *D-t* curve (D_{end}). Next, the asymmetry of the *D-t* curves was measured as the ratio E/C between the relative expansion E, defined as $(D_{\max}-D_0)/D_0$, and the relative compression C, defined as $(D_0-D_{\min})/D_0$, of the microbubble. Where $D_{\max}$ is the maximum diameter, $D_{\min}$ the minimum diameter in the *D-t* curve, and D_0 the resting diameter before vibration. The E/C ratios were used to classify the asymmetry as: 1) compression-only behavior ($E/C < 0.5$); 2) normal excursion ($0.5 \leq E/C \leq 2$); or 3) expansion-only behavior ($E/C > 2$) [29].

Using the fast Fourier transformation (FFT) the frequency content of the *D-t* curves was analyzed in terms of the amplitude at the transmit frequency (f_T). These amplitudes were fit to a resonance curve of a linear oscillator by a least-mean-squares method [6], [10] to determine the resonance frequency (f_{res}) of the microbubble. F_{res} was usually located in between two insonifications. The microbubble diameters at these insonifications are known, and the diameter at resonance D_{res} was determined from an interpolation between these two insonifications. The maximum relative radial excursions (i.e., at f_{res}) were defined as the maximum amplitude of the FFT divided by the corresponding resting diameter of the microbubble [10]. The same approach was used to determine the subharmonic resonance frequencies (f_{sub}) and the second harmonic resonance frequencies, and the corresponding maximum relative radial excursions. Next, the maximum relative radial excursions were transformed into pressures using [9], [10]

$$P_S = -\frac{\rho\omega_{\text{res}}^2 R_{\text{res}}^2 \varepsilon}{d} \tag{1}$$

where P_S is the scattered pressure at a distance d from the microbubble, $\rho = 1 \cdot 10^3$ kg/m^3 is the density of the surrounding fluid (PBS), $\omega_{\text{res}} = 2\pi f_{\text{res}}$ the angular resonance frequency, R_{res} the corresponding radius, and ε is the maximum relative radial excursion amplitude. All calculations were performed in MATLAB (The MathWorks Inc., Natick, MA, USA).

D. Statistics

Shapiro–Wilk tests for normality showed that the data was not normally distributed, so we used nonparametric testing. For comparing the acoustic stability of the microbubbles we used Wilcoxon signed-rank tests. When comparing groups, e.g., bound DSPC and nonbound DSPC, we used Mann-Whitney U tests. Medians and interquartile ranges (IQRs) are reported and were calculated using Tukey's Hinges method. Statistical analyses were performed using SPSS (Statistics 21, IBM Corporation, Armonk, NY, USA) and a p-value <0.05 was regarded as significant.

III. Results

In total, 143 single microbubbles having a D_0 between 1.5 and 10 μm were analyzed. At 50 kPa, 46 bound DPPC microbubbles were insonified; 18 of which were also insonified at 150 kPa. For bound DSPC microbubbles, 43 were

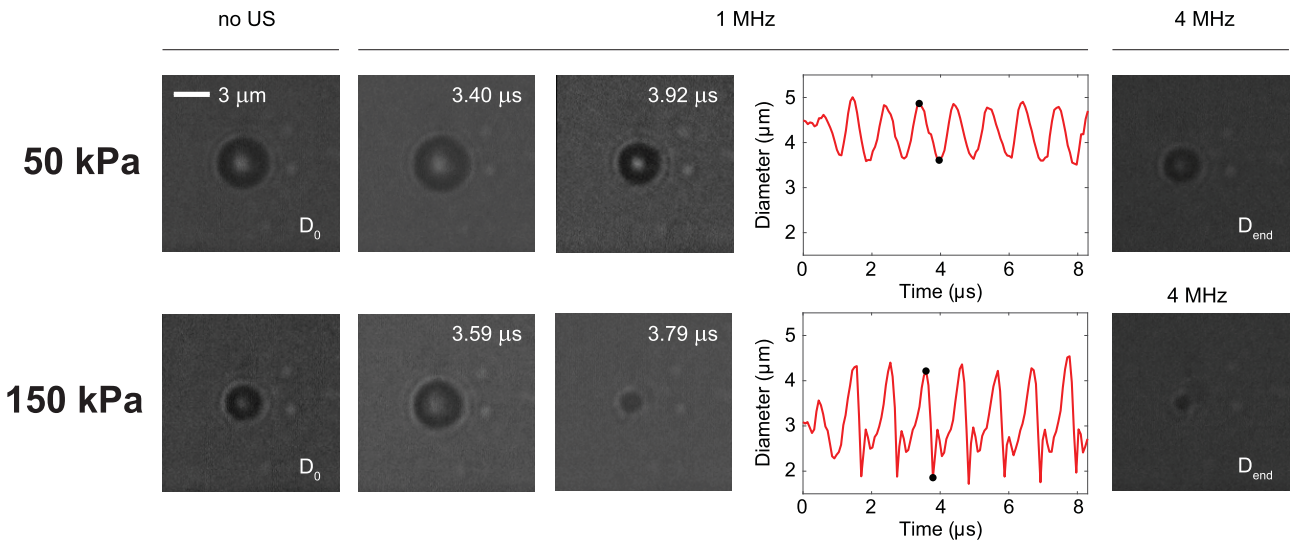

Fig. 2. Still frames of the Brandaris ultrahigh-speed recordings of a bound DPPC-based microbubble insonified at pressures of 50 and 150 kPa (see Supplemental Material for the movies). The initial state is indicated with "no US" and D_0 is determined from this recording. At a frequency of 1 MHz, two frames have been selected: one in the expansion phase and one in the compression phase of the oscillation, as also indicated by the black dots in the *D-t* curves. The curve at a pressure of 150 kPa shows inertial cavitation and thus asymmetric behavior. Acoustic deflation is clearly visible when comparing D_{end}, determined from the 4-MHz recordings, with D_0.

insonified at 50 kPa; 15 of which were also insonified at 150 kPa. None of the bound microbubbles detached during the experiments since every microbubble remained within the optic focus. For the nonbound microbubbles we included 26 DPPC and 28 DSPC microbubbles, which were all insonified at both 50 and 150 kPa.

A. Acoustic Stability

Fig. 2 shows an example of a bound DPPC-based microbubble insonified at a pressure of 50 kPa and subsequently at 150 kPa. Comparing D_0 with D_{end} at both pressures shows a clear decrease in diameter. The corresponding ultrahigh-speed Brandaris recordings can be found in the Supplementary Material, as well those of a bound DSPC-based microbubble. Overall, at $P_A = 50$ kPa, both bound DPPC and DSPC-based microbubbles deflated significantly more than when they were nonbound ($p = 0.0001$), as shown in Fig. 3. The median size for the bound DPPC microbubbles after insonification was 83% of D_0, while this was 98% for the nonbound DPPC microbubbles. The median size of bound DSPC microbubbles was 93% of D_0 after insonification, whereas nonbound DSPC microbubbles maintained their original size (100% of D_0). At a pressure of 150 kPa, the size difference between bound DPPC and nonbound DPPC microbubbles was not significant. The median diameter after insonification decreased to 53% of D_0 for bound DPPC microbubbles and to 56% for nonbound DPPC microbubbles. In case of DSPC microbubbles, those that had bound deflated more than those that had not ($p = 0.004$). For the DSPC microbubbles this was 76% for the bound ones and hardly any shrinkage (98% of their initial size) for the nonbound ones. In addition, for both bound and nonbound microbubbles, those based on DPPC deflated more than those based on DSPC at 50 kPa (bound: $p = 0.001$, nonbound: $p = 0.031$) and also at 150 kPa (both $p = 0.0001$).

B. Linear Oscillation Behavior

The resonance frequencies in relation to D_{res} are shown in Fig. 4. First of all, at a pressure of 50 kPa the resonance frequencies of bound DSPC microbubbles were similar to those of nonbound DSPC microbubbles. For DPPC-based microbubbles, the resonance frequencies of bound microbubbles were significantly higher than for nonbound DPPC microbubbles ($p = 0.045$). To further highlight the differences in resonance frequencies between bound and nonbound DPPC microbubbles, we compared the resonance frequencies of those having $D_{\text{res}} < 4$ μm. For larger microbubbles all resonance frequencies were similar, but for microbubbles having a $D_{\text{res}} < 4$ μm, the resonance frequencies of bound DPPC microbubbles were significantly higher than for nonbound DPPC microbubbles ($p = 0.002$). In addition, no overlap was found between the median (IQR) resonance frequencies of bound DPPC microbubbles and nonbound DPPC microbubbles (Table I). In contrast, the resonance frequencies of bound and nonbound DSPC microbubbles were similar for all studied sizes ($p = 0.494$). The resonance frequencies of bound DSPC microbubbles were significantly higher than those of bound DPPC-based microbubbles at $P_A = 50$ kPa ($p = 0.001$), for the nonbound DSPC and DPPC microbubbles no difference was found. All resonance frequencies at a pressure of 150 kPa were similar. The number of microbubbles included in Figs. 4 and 5 is lower than the total number of studied microbubbles, since some resonance peaks were below or above the measuring range (<1 or >4 MHz); the resonance frequency could therefore not be determined.

For bound DPPC microbubbles, the maximum relative radial excursions at a pressure of 50 kPa were significantly higher than for the nonbound DPPC microbubbles ($p = 0.002$, Fig. 5, Table I). Although the maximum relative radial excursions of bound DSPC microbubbles were not significantly different from nonbound DSPC microbubbles ($p = 0.157$) over the

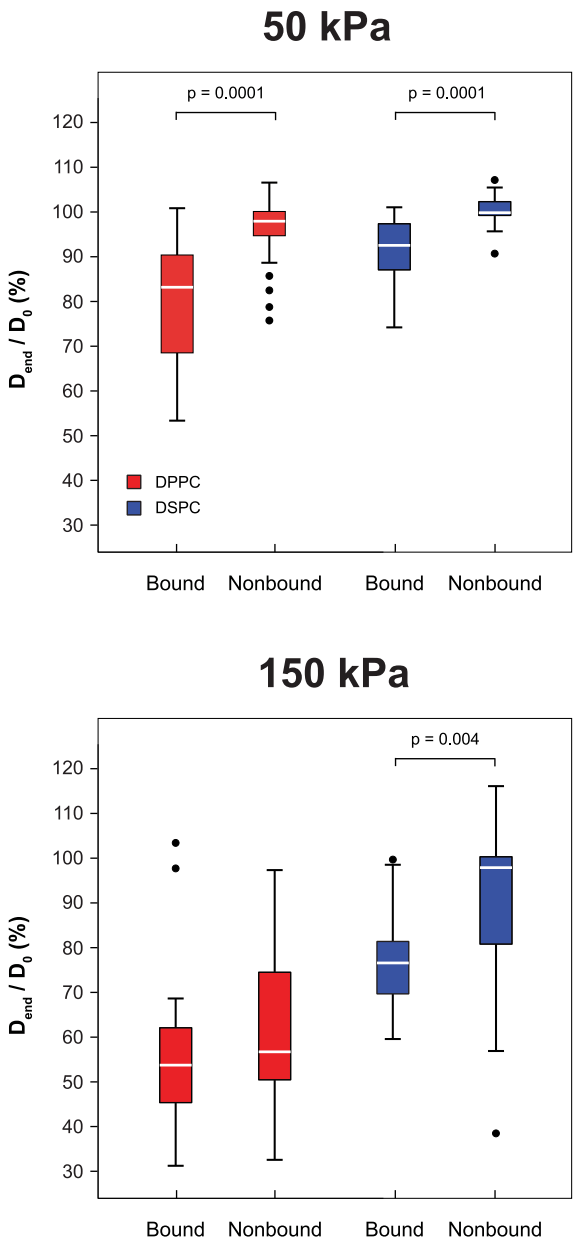

Fig. 3. Diameter change during ultrasound exposure expressed as D_0/D_{end} for bound DPPC (50 kPa: $n = 46$, 150 kPa: $n = 18$), nonbound DPPC (50 kPa: $n = 28$, 150 kPa: $n = 28$), bound DSPC (50 kPa: $n = 43$, 150 kPa: $n = 15$), and nonbound DSPC microbubbles (50 kPa: $n = 26$, 150 kPa: $n = 26$). The filled black circles are outliers.

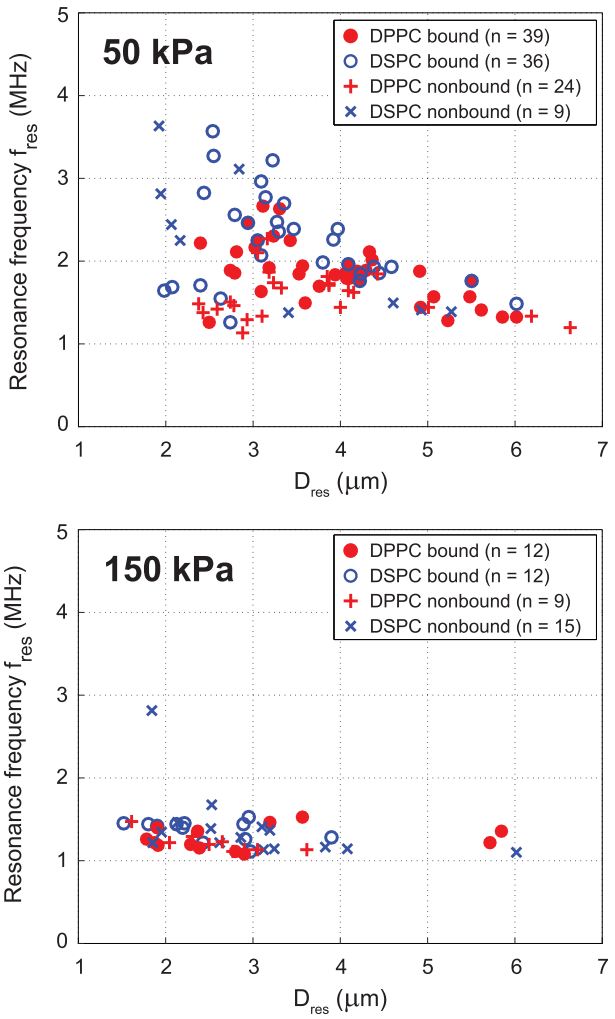

Fig. 4. Resonance frequencies (f_{res}) of bound DPPC (filled red circles), nonbound DPPC (red crosses), bound DSPC (blue open circles), and nonbound DSPC (blue crosses) microbubbles plotted versus the diameter at resonance (D_{res}) at $P_A = 50$ kPa (top panel) and $P_A = 150$ kPa (bottom panel).

whole resonance frequency range, the maximum relative radial excursions for bound DSPC microbubbles were significantly higher for resonance frequencies >2 MHz ($p = 0.001$). In addition, the maximum relative radial excursions of bound DSPC microbubbles were significantly lower than of bound DPPC microbubbles ($p = 0.0001$), but similar for the nonbound DSPC and DPPC microbubbles. At a driving pressure of 150 kPa the maximum relative radial excursions of bound and nonbound DPPC microbubbles were similar, but significantly higher for bound DSPC than nonbound DSPC microbubbles ($p = 0.001$). The maximum relative radial excursions for bound DPPC and bound DSPC-based microbubbles were similar (Fig. 5, Table I). For nonbound microbubbles the maximum relative radial excursions were significantly higher ($p = 0.03$) for DPPC microbubbles than for DSPC microbubbles.

C. Nonlinear Oscillation Behavior

The asymmetry of the radial excursions at each transmit frequency was expressed as the ratio between the relative expansion E and relative compression C. At 50 kPa, the median of the radial excursions was compression-dominated with $0.5 < E/C < 1$ for bound targeted microbubbles of both types (Fig. 6) at all frequencies. For the nonbound microbubbles the oscillations were mostly symmetric, except for the frequencies between 1 and 1.6 MHz for which the radial excursions of DPPC microbubbles were compression-dominated. At $P_A = 150$ kPa the excursion behavior of bound microbubbles at frequencies between 1 and 1.8 MHz ranged from symmetric to expansion-dominated, whereas at higher frequencies the behavior of both microbubble types was compression-dominated. An example of a bound DPPC-based microbubble showing asymmetric oscillations at 150 kPa due

TABLE I

RESONANCE FREQUENCIES AND MAXIMUM RELATIVE RADIAL EXCURSIONS PROVIDED AS MEDIAN (IQR)

Type	P_A (kPa)	Bound	D_{res} (μm)	F_{res} (MHz)	Maximum relative radial excursion
DPPC	50	Yes	1 – 7	1.85 (1.63 – 2.11)	0.14 (0.11 – 0.18)
			< 4	1.94 (1.83 – 2.25)	0.14 (0.10 – 0.20)
		No	1 – 7	1.50 (1.39 – 1.73)	0.09 (0.06 – 0.13)
			< 4	1.59 (1.40 – 1.77)	0.07 (0.06 – 0.10)
	150	Yes	1 – 7	1.22 (1.18 – 1.37)	0.28 (0.22 – 0.33)
		No	1 – 7	1.20 (1.13 – 1.24)	0.25 (0.18 – 0.28)
DSPC	50	Yes	1 – 7	2.39 (1.98 – 2.78)	0.11 (0.08 – 0.12)
			2 – 4	> 2	0.11 (0.08 – 0.12)
		No	1 – 7	2.63 (2.25 – 3.11)	0.05 (0.03 – 0.13)
			2 – 4	> 2	0.03 (0.02 – 0.04)
	150	Yes	1 – 7	1.43 (1.27 – 1.45)	0.28 (0.23 – 0.35)
		No	1 – 7	1.28 (1.15 – 1.41)	0.11 (0.09 – 0.23)

to inertial cavitation is shown in Fig. 2. The nonbound microbubbles showed mostly symmetric oscillations.

Responses at the subharmonic frequency at a driving pressure of 50 kPa were present in 22 out of 46 (48%) bound DPPC microbubbles and in 7 out of 43 (16%) bound DSPC microbubbles. For both nonbound DPPC and DSPC microbubbles only one (4%) responded at the subharmonic frequency. At the higher pressure of 150 kPa, the number of bound DPPC microbubbles responsive at the subharmonic frequency was similar to that at 50 kPa: 8 out of 18 (44%), but increased to 9 out of 15 (60%) for DSPC-based microbubbles. The number of nonbound microbubbles that responded at the subharmonic frequency increased to 12 out of 28 (43%) for DPPC and 6 out of 26 (23%) for DSPC microbubbles.

For quite some microbubbles a response at the subharmonic frequency was observed in the FFT of the *D-t* curves. However, to determine the scattered subharmonic pressures using (1), the subharmonic resonance frequency f_{sub} is required; f_{sub} could only be determined for the microbubbles shown in Fig. 7. Reasons for not being able to determine the subharmonic resonance curve were not enough points for a fit or the peak of the subharmonic resonance curve was below or above the measuring range. Emitted subharmonic pressures at a distance of 2 cm were similar irrespective of binding and the type of lipid coating at each acoustic pressure (Fig. 7), but their origin was different. At 50 kPa, of the 17 bound DPPC microbubbles shown in Fig. 7, nine had a response at transmit at twice the resonance frequency (T2R with $f_{sub} = f_{res}$ [30], [31]) and four at transmit at the resonance frequency (TR, $f_{sub} = 1/2\ f_{res}$ [8], [30]). Of the seven bound DSPC microbubbles, three had a clear response at T2R and none

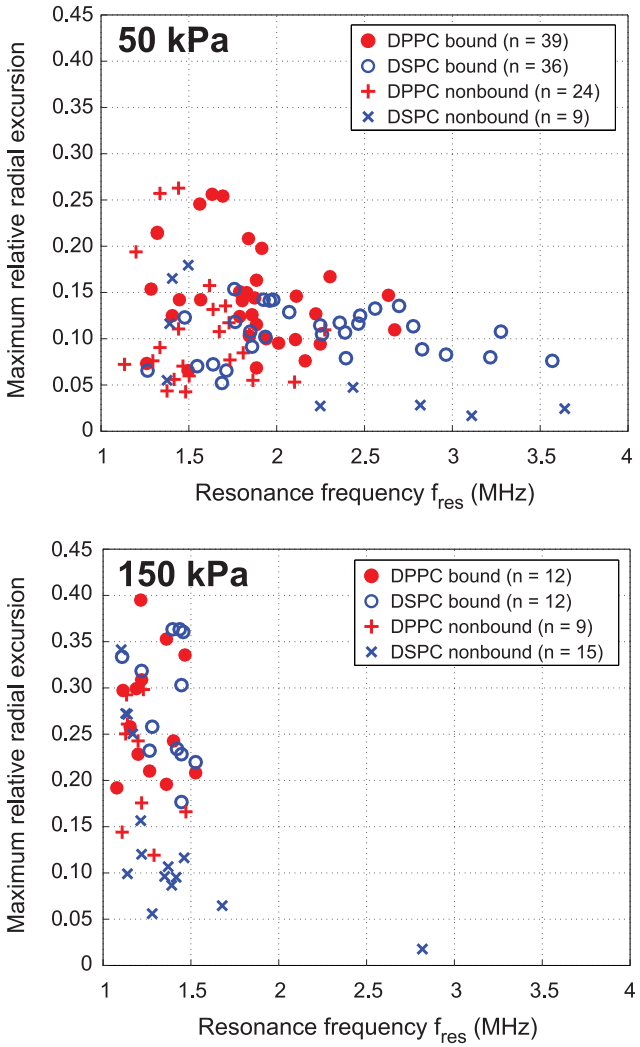

Fig. 5. Maximum relative radial excursions at the resonance frequency of bound DPPC (filled red circles) nonbound DPPC (red crosses), bound DSPC (blue open circles), and nonbound DSPC (blue crosses) microbubbles plotted versus the resonance frequency (f_{res}) at $P_A = 50$ kPa (top panel) and $P_A = 150$ kPa (bottom panel).

had a response at TR. At 150 kPa, of the eight bound DPPC microbubbles seven had a response at T2R and one at TR. Of the seven bound DSPC microbubbles four had a response at T2R and none at TR. In the case of nonbound microbubbles at 50 kPa the only microbubble responsive at f_{sub} was a DSPC microbubble with a response at T2R. At 150 kPa, one out of the ten DPPC microbubbles had a response at T2R and two out of ten at TR. For the four nonbound DSPC microbubbles two had a response at T2R and none at TR. For the other microbubbles responding at f_{sub}, the relation between TR or T2R could not be determined; either because no clear relation was found between the subharmonic and fundamental frequency, or because the fundamental frequency had not been determined since the peak was located outside the measuring range. We assumed a detection limit of 1 Pa (black dashed line in Fig. 7) for diagnostic ultrasound scanners, achievable with a typical high-quality transducer for harmonic imaging [32].

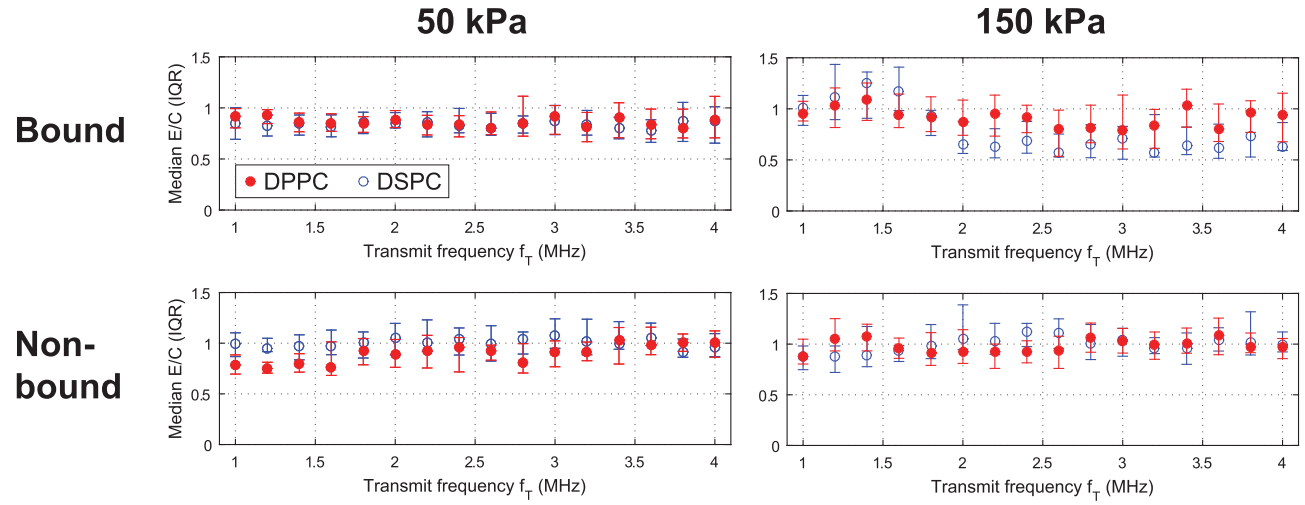

Fig. 6. Median (IQR) ratio between the relative expansion E and the relative compression C of bound DPPC (50 kPa: $n = 37$, 150 kPa: $n = 18$) and bound DSPC (50 kPa: $n = 43$, 150 kPa: $n = 15$) microbubbles (top panels), and nonbound DPPC (50 kPa: $n = 28$, 150 kPa: $n = 28$) and nonbound DSPC (50 kPa: $n = 26$, 150 kPa: $n = 26$) microbubbles (bottom panels) plotted versus the transmit frequency at $P_A = 50$ kPa (left panels) and $P_A = 150$ kPa (right panels).

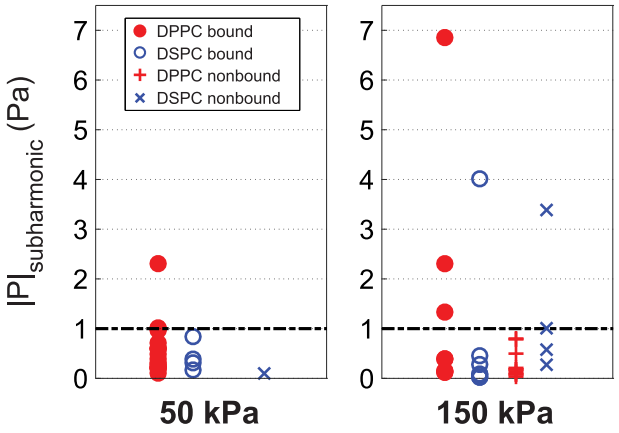

Fig. 7. Absolute pressures emitted at the subharmonic resonance frequency of bound DPPC (50 kPa: $n = 17$, 150 kPa: $n = 8$), bound DSPC microbubbles (50 kPa: $n = 7$, 150 kPa: $n = 7$), nonbound DPPC (50 kPa: $n = 0$, 150 kPa: $n = 10$), and nonbound DSPC microbubbles (50 kPa: $n = 1$, 150 kPa: $n = 4$).

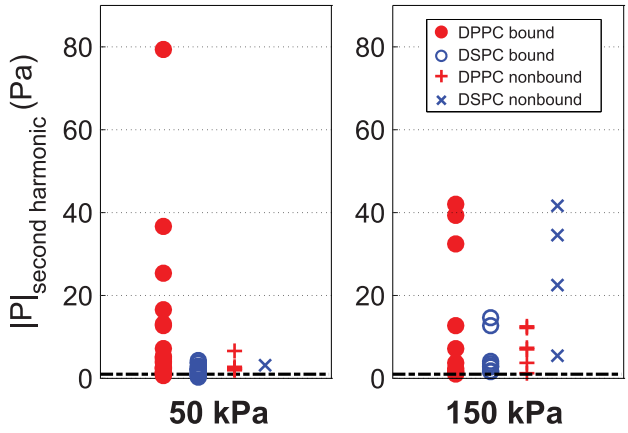

Fig. 8. Absolute pressures emitted at the second harmonic resonance frequency of bound DPPC (50 kPa: $n = 21$, 150 kPa: $n = 10$), bound DSPC microbubbles (50 kPa: $n = 19$, 150 kPa: $n = 8$), nonbound DPPC (50 kPa: $n = 6$, 150 kPa: $n = 6$), and nonbound DSPC microbubbles (50 kPa: $n = 1$, 150 kPa: $n = 4$).

At $P_A = 50$ kPa, about half of both bound DPPC (53%) and bound DSPC (57%) microbubbles responded at the second harmonic frequency. The number of responding nonbound microbubbles based on DPPC was similar (50%), but for nonbound DSPC microbubbles only 1 out of 26 (4%) was responsive at the second harmonic frequency. The number of responsive microbubbles at a driving pressure of 150 kPa increased in all cases: to 14 out of 15 (93%) for bound DPPC, 13 out of 18 (72%) for bound DSPC, 17 out of 28 (61%) for nonbound DPPC, and 8 out of 26 (31%) for nonbound DSPC microbubbles. The median (IQR) pressures emitted at the second harmonic frequency when insonified at 50 kPa were 2.0 (1.0–2.6) Pa for bound DSPC microbubbles, hence in the same order as the only nonbound DSPC microbubble (3.1 Pa, Fig. 8). For bound and nonbound DPPC microbubbles, the emitted pressures were not significantly different ($p = 0.351$). In addition, the emitted pressures at the second harmonic frequency of bound DPPC microbubbles were higher than those of bound DSPC microbubbles ($p = 0.004$). At the higher driving pressure of 150 kPa, the emitted pressures were significantly higher ($p = 0.017$) for nonbound than bound DSPC microbubbles, with median pressures of 28.5 (14.0–38.1) Pa for nonbound and 3.2 (2.4–8.4) Pa for bound DSPC microbubbles. The median pressures of the other groups were all similar.

IV. Discussion

This paper investigated vibrational responses of bound and nonbound microbubbles to identify differences to acoustically discriminate them. For DPPC-based microbubbles with diameters between 2 and 4 μm the resonance frequencies and relative radial excursions were higher than for nonbound DPPC-based microbubbles ($P_A = 50$ kPa). In contrast, at an insonifying pressure of 150 kPa the relative radial excursions for bound and nonbound DPPC-based microbubbles were similar. Interestingly, at this higher pressure the radial excursions

for bound DSPC-based microbubbles were higher than for nonbound DSPC microbubbles, whereas these were similar at 50 kPa. We also found compression-dominated behavior and a higher number of responsive microbubbles at the second harmonic frequency for bound microbubbles, irrespective of the main coating lipid.

A. Acoustic Stability

Bound microbubbles were acoustically less stable than nonbound microbubbles, irrespective of their main coating component. Further, we found that the acoustic stability for DPPC-based microbubbles was lower than that for DSPC-based microbubbles. This was previously attributed to the shorter acyl chain length of the DPPC lipid than that of the DSPC lipid [10]. This shorter chain results in lower intermolecular van der Waals forces between the different lipids and results in less attraction and cohesion of the microbubble shell [10], [33]. The maximum relative radial excursions of bound microbubbles were higher at the resonance frequency than those of nonbound microbubbles (for DPPC at 50 kPa and DSPC at 150 kPa). This means that the radial excursions after binding were more prominent, which resulted in more shrinkage and therefore a lower acoustic stability. Others have reported lower radial excursions after binding for DSPC-based microbubbles [12], [14], but those studies had not covalently linked their model biomarker to their membrane. As a result, the biomarker that attached to the microbubble shell increased the stiffness [20] and therefore limits the radial oscillations.

Some nonbound DSPC microbubbles appeared to increase in diameter after insonification at 150 kPa. The microbubbles in which this was observed were all relatively small ($<$2.5 μm). This apparent increase may be due to small changes in the optic focus due to radiation forces, in combination with the error in the tracking algorithm which was previously estimated to be approximately 10% [6].

B. Linear Oscillation Behavior

The resonance frequencies for bound DPPC microbubbles were higher than for nonbound DPPC microbubbles at a pressure of 50 kPa for microbubbles with diameters between 2 and 4 μm at resonance. Based on the IQRs, the resonance frequencies of most bound DPPC microbubbles of this size were higher than 1.8 MHz, whereas those of nonbound DPPC microbubbles were lower than 1.8 MHz. In terms of shell properties, a higher resonance frequency is related to an increase in elasticity (i.e., a stiffer shell) by the Marmottant model [34]. It is not likely that the elasticity changes upon binding, but the apparent stiffness may increase due to binding of the microbubble to the biomarker. We may not have found a change in apparent stiffness for DSPC-based microbubbles, because their surface binding area is smaller than for DPPC-based microbubbles as previously determined by our group for the same type of microbubbles and same streptavidin biomarker [21]. Next, the initial elasticity of DSPC microbubbles is already higher than for DPPC microbubbles [10], and it has been shown that the resonance frequencies for DSPC microbubbles did not change after conjugating the relatively heavy molecule streptavidin to the lipid shell, whereas for DPPC microbubbles the resonance frequencies increased [20]. In addition, the resonance frequency exponentially decreases for increasing microbubble size [35]. As a consequence, the difference in resonance frequencies for microbubbles with diameters between 2 and 4 μm is larger than for microbubbles with diameters between 5 and 7 μm [10]. An increase in resonance frequency for bound microbubbles will therefore be more pronounced for smaller than for larger microbubbles. This may explain why the apparent increase in stiffness was only present for bound DPPC microbubbles having diameters between 2 and 4, and not for DSPC microbubbles or larger DPPC microbubbles. At 150 kPa, however, all resonance frequencies appeared the same. The microbubble oscillations at this pressure start off very violently (i.e., inertial cavitation) in the first insonifications between 1 and 1.5 MHz, thereby largely decreasing the microbubble size and shifting its original resonance frequency toward higher frequencies. Since the mechanical index was $\sim$2$\times$ lower for the insonifications at the end of the frequency sweep, the resulting relative radial excursions were lower at the new resonant microbubble size. Therefore, the oscillations of the first insonifications dominated the resonance behavior, leading to an apparent resonance frequency between 1 and 1.5 MHz before shrinkage.

Others have also reported differences in resonance frequencies between bound and nonbound microbubbles. Casey *et al.* [15] reported an increase in resonance frequency for their bound in-house produced biotinylated microbubbles, but for DSPC microbubbles (C_3F_8 gas core and same components as our DSPC-based microbubbles, but unknown ratios) instead of for DPPC-based microbubbles as we report here. Overvelde *et al.* [12] found 30% lower frequencies of maximum response for targeted BG-6438 microbubbles bound to an OptiCell wall than for nontargeted BG-6437 microbubbles floating against the wall at pressures $<$40 kPa (both bubble types are from Bracco Research S.A., Geneva, Switzerland). The BG-6438 microbubbles were targeted to FITC-BSA using an anti-FITC antibody attached to the microbubble shell using streptavidin-biotin bridging. The main limitation of both studies is the method of attaching the model biomarker streptavidin to the cellulose tube [15] or FITC-BSA to the OptiCell wall [12], namely, by physisorption. As mentioned before, this physisorbed biomarker is likely to bind to the microbubble shell creating a lipid-coated microbubble covered with the model biomarker. These very large and heavy complexes are expected to behave completely different in an ultrasound field than a bare lipid-coated targeted microbubble, as has been shown for microbubbles that were functionalized with streptavidin, depending on the initial stiffness of the microbubble coating [20]. In addition to this, Overvelde *et al.* [12] did not block the OptiCells to prevent unspecific binding in their experiments that compared free BG-6437 microbubbles and BG-6437 microbubbles close to the wall: the latter may have actually bound to the wall. Next to that, the BG-6437 microbubbles did not have anti-FITC antibody attached to their shell, which is not a fair comparison between microbubbles that have bound to the wall

and that are floating against the wall. In our present study, the covalent coupling of streptavidin to the hydrogel, and thus the membrane, was established and it was confirmed that no streptavidin was present on the microbubble shell [21].

C. Nonlinear Oscillation Behavior

For nonlinear contrast-enhanced ultrasound imaging the responses at the subharmonic and second harmonic frequencies are usually exploited [36]. At 50 kPa more bound than nonbound microbubbles responded at the subharmonic frequency, for both the DPPC and DSPC-based coatings. At 150 kPa more microbubbles—both bound and nonbound—were responsive at the subharmonic frequency, but the emitted pressures of single microbubbles were close to or below the assumed detection limit for clinical use of 1 Pa [32]. Based on these results, the subharmonic emissions seem of limited use for nonlinear contrast-enhanced imaging and discrimination of bound from nonbound microbubble based on our experimental conditions. However, when multiple microbubbles are in close proximity of each other, their subharmonic emissions could be in phase and the resulting cumulative pressure may be higher [13]. This is worth to further investigate, but was outside the scope of this paper.

We found similar amplitudes at the subharmonic frequency for bound and nonbound microbubbles, in line with the findings of Zhao *et al.* [14] for microbubbles with a coating of 82 mol% DSPC, 9 mol% DSPE-PEG(2000), and 9 mol% DSPE-PEG(2000)-biotin [37]. Helfield *et al.* [13] reported similar amounts of bound and nonbound Target-Ready MicroMarker microbubbles that were responsive at the subharmonic frequency, whereas we found more bound microbubbles that responded. The different composition and gas core of Target-Ready MicroMarker likely contributed to these differences. As suggested in [13], the membrane material could have frequency-dependent effects and their results might be biased due to aggregation of microbubbles that may have changed the echogenicity [38]. We previously performed the exact same experiments as described here for nonbound microbubbles in an OptiCell [39]. Indeed, a membrane dependent effect was observed, but was not found to be frequency related. The maximum relative radial excursions of nonbound microbubbles in an OptiCell (both DPPC and DSPC) were 2–2.5 times higher than for nonbound microbubbles floating against the hydrogel. Because the microbubbles may be partly embedded in the polymer-based hydrogel, this can damp the microbubble oscillations and therefore result in lower maximum relative radial excursions.

Another difference between our study and that in [13] is that they coated their cellulose tube with streptavidin using physisorption, with the disadvantage of streptavidin covering the microbubble shell, which may have influenced the amplitude of the subharmonic signal. Indeed, their acoustic measurements showed a 20% higher subharmonic signal of Target-Ready MicroMarker, a streptavidin-functionalized lipid-coated microbubble, when bound to a biotinylated agarose phantom. The difference between the results in [13] and our results presented in this paper might also be due to the used techniques: ultrahigh-speed optical imaging versus acoustic measurements. In our setup, we were only able to image the top-view of the microbubble oscillations, whereas acoustic measurements can detect out-of-plane signals as well. If a larger portion of the subharmonic excursions were generated in the perpendicular plane, we might have missed those vibrations with our setup.

Numerical simulations have shown that the subharmonic signal is optimal when the microbubble is insonified at T2R [40]. Experimental validation showed that the threshold for generating TR subharmonic responses is higher than that for T2R subharmonic responses in lipid-coated microbubbles [30], [41]. The absence of DSPC responders at TR may suggest that the threshold for generating TR subharmonic responses is lower for DPPC microbubbles than for DSPC microbubbles, irrespective of them being bound or not. On the other hand, due to the applied frequency range and studied microbubble sizes, the majority of the resonance frequencies were between 1.5 and 3.5 MHz; this limits the possibility to insonify microbubbles at T2R within the frequency range we applied.

The higher second harmonic amplitudes we measured for nonbound DSPC-based microbubbles at 150 kPa are in contrast with results reported by others [11], [15]. The study in [15] used microbubbles similar to our DSPC microbubbles, but with a C_3F_8 core and attachment to a capillary wall using the physisorbed streptavidin as biomarker ($f_T = 2$ MHz, $P_A = 90$ kPa). The study in [11] also used DSPC-based microbubbles, with a setup and parameters comparable to those in [15]. Both studies used somewhat lower pressures, but may also have effectively studied bound targeted DSPC-based microbubbles coated with a streptavidin layer, which may explain the different findings. In our study, the emitted pressure amplitudes of bound microbubbles were similar or lower than for nonbound microbubbles and acoustic discrimination based on the second harmonic pressures does therefore not seem feasible.

D. DSPC Versus DPPC for Ultrasound Molecular Imaging Applications

The differences between bound targeted DPPC and DSPC-based microbubbles were not as pronounced as we expected from the differences in shape change upon adherence and their surface binding areas, as previously determined by our group for the same type of microbubbles and same streptavidin biomarker [21]. The most prominent differences we did find were higher acoustic stability for nonbound microbubbles, higher resonance frequencies (for DPPC microbubbles with diameters between 2 and 4 μm) and radial excursions for bound DPPC microbubbles at 50 kPa, and higher amplitudes at the second harmonic frequency for nonbound DSPC microbubbles than for bound DSPC microbubbles at 150 kPa. The lower resonance frequencies for DPPC microbubbles than for DSPC microbubbles were already observed for nonbound DPPC microbubbles [10], and were thus maintained upon binding.

For *in vivo* ultrasound molecular imaging the ideal targeted microbubble: 1) can effectively bind to the biomarker of interest; 2) persists binding to the biomarker after initial

binding, i.e., the binding strength is larger than the shear stress induced by the flowing blood; 3) is stable during the course of the ultrasound examination; 4) nonlinearly scatters ultrasound that is microbubble specific; 5) can be discriminated acoustically from nonbound microbubbles; and 6) has the same resonance frequency as the other microbubbles that are injected, i.e., all microbubbles in the population respond in the same way to ultrasound. Concerning the first two points, Kooiman *et al.* [21] favored targeted DPPC microbubbles over DSPC microbubbles because of their larger surface binding area to a streptavidin-coated membrane, their dome shape after binding, and a more homogeneous distribution of fluorescently labeled ligands attached to DSPE-PEG(2000). The more homogeneous lipid distribution might aid the initial attachment, whereas the larger binding area and difference in shape might be able to better sustain blood shear forces. However, binding of the microbubbles was performed under static conditions and experiments in the presence of flow are required to verify which of the two microbubble types binds best under flow. Based on the acoustic stability (point 3), DSPC-based microbubbles are favored over DPPC-based microbubbles. This also means that the size is better maintained during insonification and the resonance frequency will therefore be more consistent throughout the investigation. In terms of nonlinear scattering of ultrasound (point 4), the maximum relative radial excursions at the subharmonic frequency for both our DPPC and DSPC microbubbles resulted in $\sim$20 dB lower scattered pressures than the second harmonic responses. The subharmonic responses were unpredictable and too low to discriminate bound from nonbound microbubbles. In contrast, the responses at the second harmonic frequency were sufficiently high to be detected, but amplitudes were similar for bound and nonbound microbubbles, or higher for the nonbound ones in terms of DSPC-based microbubbles (point 5). At 50 kPa, bound and nonbound DPPC microbubbles with diameters between 2 and 4 μm at resonance could be separated based on their resonance frequencies: bound DPPC microbubbles had resonance frequencies above 1.8 MHz, whereas those were significantly lower for nonbound DPPC microbubbles. Lastly (point 6), as mentioned in the introduction one of the main challenges for successful translation of ultrasound molecular imaging to the clinic is the production of microbubble populations that have the same acoustic signature. Both the DPPC and DSPC-based microbubbles can have different resonance frequencies and radial excursions although their sizes are similar. Several studies showed that monodisperse lipid-coated microbubble distributions can be produced using flow-focusing devices [42]–[45]. Kaya *et al.* [43] and Talu *et al.* [45] studied the difference between echo amplitudes of these monodisperse single microbubbles when insonified at a frequency close to resonance, and found a lower standard deviation than for polydisperse microbubbles. Segers and Versluis [46] developed an acoustic sorting chip that separated monodisperse microbubbles based on the radiation force they experienced, which resulted in an overall contrast enrichment of more than 10 dB. This is an important step toward improving the quality of *in vivo* ultrasound molecular imaging, especially if microbubbles with low shell elasticity and a diameter between 2 and 4 μm can be produced to distinguish bound from nonbound microbubbles, as shown in our study. However, this approach is still limited to specific microbubble compositions that can be produced monodispersely by means of flow-focusing devices.

Summing up all the aforementioned similarities, differences, advantages, and disadvantages of DPPC and DSPC-based microbubbles, this results in a favor for DSPC-based microbubbles for ultrasound molecular imaging, solely based on a higher acoustic stability. Studying the adherence of the microbubbles under flow should reveal whether the heterogeneous lipid distribution in the DSPC shell hinders binding. On the other hand, bound DPPC microbubbles (diameters between 2 and 4 μm) at 50 kPa had resonance frequencies higher than 1.8 MHz, whereas those of nonbound DPPC microbubbles were lower than 1.8 MHz. In addition, the relative radial excursions of bound DPPC microbubbles were also higher. When monodisperse DPPC microbubbles with a diameter between 2 and 4 μm are produced, these could acoustically be discriminated based on their resonance frequency.

E. Limitations and Outlook

Although we aimed to create a more *in vivo*-like setup using covalent biomarker binding versus physisorption, the membrane we used in our experiments was still artificial. The 1–2-μm-thick hydrogel created a softer layer between the microbubble and the polyester membrane, but to have a real *in vivo*-like membrane one would need to develop a material with exactly the same stiffness, viscosity, etc. as an actual cell layer or perform *in vivo* experiments. In addition, *in vivo* one can also study microbubble vibration when microbubbles are in contact with cells and under flow, for which the chorioallantoic membrane model could be used. This model has proven to be useful to study nontargeted microbubble vibration using ultrahigh-speed imaging and targeted-microbubble mediated drug delivery [47], [48].

For *in vivo* ultrasound molecular imaging multiple microbubbles may bind in closer range with each other than investigated in this paper. However, the binding range actually depends on the availability of the biomarker on the cell surface, which depends both on the cell type and the biomarker of interest. When the interbubble distance is $\leq$10 μm, this will cause interaction of the bubbles in terms of secondary Bjerknes forces, and due to the secondary Bjerknes forces a bubble will deform in the direction of their neighboring bubble [49]. Next to that, two similar sized bubbles that are close to each other result in a shift in resonance frequency and therefore a decrease in maximum relative radial excursions [50]. As a consequence, for abundant biomarkers on the cell membrane these observations may counteract the increase in resonance frequency and maximum relative radial excursions we observed for DPPC microbubbles between 2 and 4 μm at 50 kPa. This, however, should first be experimentally verified using a setup comprising of a biomarker distribution that is comparable to the *in vivo* situation. The chorioallantoic model would be a good approach to study this.

V. Conclusion

This paper shows that binding of in-house produced DPPC-based microbubbles to a streptavidin-coated surface increased the resonance frequencies (for microbubbles with diameters between 2 and 4 μm) and the corresponding relative radial excursions at relatively low pressure (50 kPa). At this pressure, the bound 2- to 4-μm microbubbles resonated above 1.8 MHz, whereas the nonbound 2- to 4-μm DPPC microbubbles were resonant below this frequency. In terms of nonlinear responses, only the responses at the second harmonic frequency of bound DSPC microbubbles at 150 kPa were lower than of nonbound DSPC microbubbles. Our in-house produced DSPC-based microbubbles were acoustically more stable than our DPPC-based microbubbles, which is the major advantage of this type of microbubble for ultrasound molecular imaging applications.

Acknowledgment

The authors would like to thank R. Beurskens, F. Mastik, M. Manten, and G. Springeling for technical assistance, Dr. T. Kokhuis for valuable discussions (all from the Department of Biomedical Engineering, Thorax Center, Erasmus MC), and Dr. J. L. Raymond for experimental assistance (visiting fellow Whitaker program). They would also like to thank I. Chrifi from the Department of Experimental Cardiology, Thorax Center, Erasmus MC, for the spectrophotometer measurements, and Dr. E. Gedig from XanTec bioanalytics GmbH, Germany, for discussions about the covalent coating of streptavidin to the polyester membranes. The authors are grateful to Prof. Dr. A. L. Klibanov from the University of Virginia, Cardiovascular Division, Charlottesville, VA, USA, for discussions about the microbubble preparation.

References

[1] A. Alzaraa *et al.*, "Targeted microbubbles in the experimental and clinical setting," *Amer. J. Surgery*, vol. 204, pp. 355–366, Sep. 2012.

[2] J. S.-M. Yeh *et al.*, "Quantitative ultrasound molecular imaging," *Ultrasound Med. Biol.*, vol. 41, no. 9, pp. 2478–2496, Sep. 2015.

[3] L. Abou-Elkacem, S. V. Bachawal, and J. K. Willmann, "Ultrasound molecular imaging: Moving toward clinical translation," *Eur. J. Radiol.*, vol. 84, no. 9, pp. 1685–1693, Sep. 2015.

[4] F. Kiessling, S. Fokong, J. Bzyl, W. Lederle, M. Palmowski, and T. Lammers, "Recent advances in molecular, multimodal and theranostic ultrasound imaging," *Adv. Drug Delivery Rev.*, vol. 72, pp. 15–27, Jun. 2014.

[5] A. L. Klibanov, "Ultrasound contrast materials in cardiovascular medicine: From perfusion assessment to molecular imaging," *J. Cardiovascular Transl. Res.*, vol. 6, no. 5, pp. 729–739, Oct. 2013.

[6] S. M. van der Meer *et al.*, "Microbubble spectroscopy of ultrasound contrast agents," *J. Acoust. Soc. Amer.*, vol. 121, pp. 648–656, Jan. 2007.

[7] Y. Luan *et al.*, "Acoustical properties of individual liposome-loaded microbubbles," *Ultrasound Med. Biol.*, vol. 38, pp. 2174–2185, Dec. 2012.

[8] T. Faez, M. Emmer, M. Docter, J. Sijl, M. Versluis, and N. de Jong, "Characterizing the subharmonic response of phospholipid-coated microbubbles for carotid imaging," *Ultrasound Med. Biol.*, vol. 37, pp. 958–970, Jun. 2011.

[9] M. Emmer, H. J. Vos, M. Versluis, and N. de Jong, "Radial modulation of single microbubbles," *IEEE Trans. Ultrason., Ferroelect., Freq. Control*, vol. 56, no. 11, pp. 2370–2379, Nov. 2009.

[10] T. van Rooij *et al.*, "Non-linear response and viscoelastic properties of lipid-coated microbubbles: DSPC versus DPPC," *Ultrasound Med. Biol.*, vol. 41, pp. 1432–1445, May 2015.

[11] S. Zhao, D. E. Kruse, K. W. Ferrara, and P. A. Dayton, "Acoustic response from adherent targeted contrast agents," *J. Acoust. Soc. Amer.*, vol. 120, pp. EL63–EL69, Dec. 2006.

[12] M. Overvelde, V. Garbin, B. Dollet, N. de Jong, D. Lohse, and M. Versluis, "Dynamics of coated microbubbles adherent to a wall," *Ultrasound Med. Biol.*, vol. 37, pp. 1500–1508, Sep. 2011.

[13] B. L. Helfield, E. Cherin, F. S. Foster, and D. E. Goertz, "The effect of binding on the subharmonic emissions from individual lipid-encapsulated microbubbles at transmit frequencies of 11 and 25 MHz," *Ultrasound Med. Biol.*, vol. 39, pp. 345–359, Feb. 2013.

[14] S. Zhao, K. W. Ferrara, and P. A. Dayton, "Asymmetric oscillation of adherent targeted ultrasound contrast agents," *Appl. Phys. Lett.*, vol. 87, pp. 1341031–1341033, Sep. 2005.

[15] J. Casey, C. Sennoga, H. Mulvana, J. V. Hajnal, M. X. Tang, and R. J. Eckersley, "Single bubble acoustic characterization and stability measurement of adherent microbubbles," *Ultrasound Med. Biol.*, vol. 39, pp. 903–914, May 2013.

[16] D. Kim and A. E. Herr, "Protein immobilization techniques for microfluidic assays," *Biomicrofluidics*, vol. 7, no. 4, p. 41501, 2013.

[17] K. Kooiman *et al.*, "Surface contact of bound targeted microbubbles," in *Proc. IEEE Ultrasonics Symp.*, Dresden, Germany, Oct. 2012, pp. 2161–2163.

[18] R. H. Abou-Saleh, S. A. Peyman, K. Critchley, S. D. Evans, and N. H. Thomson, "Nanomechanics of lipid encapsulated microbubbles with functional coatings," *Langmuir*, vol. 29, pp. 4096–4103, Mar. 2013.

[19] J. E. McKendry, C. A. Johnson, B. R. G. Coletta, P. L. Evans, J. A. Evans, and S. D. Evans, "Force spectroscopy of streptavidin conjugated lipid coated microbubbles," *Bubble Sci., Eng. Technol.*, vol. 2, no. 2, pp. 48–54, 2010.

[20] T. van Rooij, V. Daeichin, I. Skachkov, N. de Jong, and K. Kooiman, "Targeted ultrasound contrast agents for ultrasound molecular imaging and therapy," *Int. J. Hyperthermia*, vol. 31, pp. 90–106, Feb. 2015.

[21] K. Kooiman *et al.*, "DSPC or DPPC as main shell component influences ligand distribution and binding area of lipid-coated targeted microbubbles," *Eur. J. Lipid Sci. Technol.*, vol. 116, pp. 1217–1227, Sep. 2014.

[22] Lantheus Medical Imaging, "Definity safety label," FDA/Center Drug Eval. Res., Silver Spring, USA, Tech. Rep. 3910678, Oct. 2011.

[23] M. Schneider *et al.*, "BR1: A new ultrasonographic contrast agent based on sulfur hexafluoride-filled microbubbles," *Invest Radiol.*, vol. 30, pp. 451–457, Aug. 1995.

[24] M. Schneider *et al.*, "Gray-scale liver enhancement in VX2 tumor-bearing rabbits using BR14, a new ultrasonographic contrast agent," *Invest. Radiol.*, vol. 32, pp. 410–417, Jul. 1997.

[25] Bracco Diagnostics Inc, "Lumason safety label," FDA/Center Drug Eval. Res., Silver Spring, USA, Tech. Rep. 3033313, Mar. 2016.

[26] T. C. Chin *et al.*, "Brandaris 128: A digital 25 million frames per second camera with 128 highly sensitive frames," *Rev. Sci. Instrum.*, vol. 74, pp. 5026–5034, Dec. 2003.

[27] A. L. Klibanov *et al.*, "Detection of individual microbubbles of ultrasound contrast agents: Imaging of free-floating and targeted bubbles," *Invest. Radiol.*, vol. 39, pp. 187–195, Mar. 2004.

[28] E. C. Gelderblom *et al.*, "Brandaris 128 ultra-high-speed imaging facility: 10 Years of operation, updates, and enhanced features," *Rev. Sci. Instrum.*, vol. 83, p. 103706, Oct. 2012.

[29] N. de Jong *et al.*, "'Compression-only' behavior phospholipid-coated contrast bubbles," *Ultrasound Med. Biol.*, vol. 33, pp. 653–656, Apr. 2007.

[30] J. Chomas, P. Dayton, D. May, and K. Ferrara, "Nondestructive subharmonic imaging," *IEEE Trans. Ultrason., Ferroelectr., Freq. Control*, vol. 49, no. 7, pp. 883–892, Jul. 2002.

[31] J. Sijl *et al.*, "Subharmonic behavior of phospholipid-coated ultrasound contrast agent microbubbles," *J. Acoust. Soc. Amer.*, vol. 128, pp. 3239–3252, Nov. 2010.

[32] P. L. M. J. Van Neer, G. Matte, M. G. Danilouchkine, C. Prins, F. Van Den Adel, and N. De Jong, "Super-harmonic imaging: Development of an interleaved phased-array transducer," *IEEE Trans. Ultrason., Ferroelect., Freq. Control*, vol. 57, no. 2, pp. 455–468, Feb. 2010.

[33] D. H. Kim, M. J. Costello, P. B. Duncan, and D. Needham, "Mechanical properties and microstructure of polycrystalline phospholipid monolayer shells: Novel solid microparticles," *Langmuir*, vol. 19, pp. 8455–8466, Sep. 2003.

[34] P. Marmottant *et al.*, "A model for large amplitude oscillations of coated bubbles accounting for buckling and rupture," *J. Acoust. Soc. Amer.*, vol. 118, pp. 3499–3505, Dec. 2005.

[35] M. Minnaert, "XVI. On musical air-bubbles and the sounds of running water," *London, Edinburgh, Dublin Philos. Mag. J. Sci.*, vol. 16, no. 104, pp. 235–248, 1933.

[36] A. Needles *et al.*, "Nonlinear contrast imaging with an array-based micro-ultrasound system," *Ultrasound Med. Biol.*, vol. 36, pp. 2097–2106, Dec. 2010.

[37] S. Zhao, M. Borden, S. H. Bloch, D. Kruse, K. W. Ferrara, and P. A. Dayton, "Radiation-force assisted targeting facilitates ultrasonic molecular imaging," *Molecular Imag.*, vol. 3, pp. 135–148, Jul. 2004.
[38] P. A. Dayton, K. E. Morgan, A. L. Klibanov, G. H. Brandenburger, and K. W. Ferrara, "Optical and acoustical observations of the effects of ultrasound on contrast agents," *IEEE Trans. Ultrason., Ferroelectr., Freq. Control*, vol. 46, no. 1, pp. 220–232, Jan. 1999.
[39] T. van Rooij, A. F. W. van der Steen, N. de Jong, and K. Kooiman, "Influence of binding on the vibrational responses of targeted lipid-coated microbubbles," in *Proc. IEEE Int. Ultrasonics Symp. Proceedings*, Chicago, IL, USA, Sep. 2014, pp. 413–416.
[40] P. M. Shankar, P. D. Krishna, and V. L. Newhouse, "Subharmonic backscattering from ultrasound contrast agents," *J. Acoust. Soc. Amer.*, vol. 106, pp. 2104–2110, Oct. 1999.
[41] P. M. Shankar, P. D. Krishna, and V. L. Newhouse, "Advantages of subharmonic over second harmonic backscatter for contrast-to-tissue echo enhancement," *Ultrasound Med. Biol.*, vol. 24, pp. 395–399, Mar. 1998.
[42] K. Hettiarachchi, E. Talu, M. L. Longo, P. A. Dayton, and A. P. Lee, "On-chip generation of microbubbles as a practical technology for manufacturing contrast agents for ultrasonic imaging," *Lab Chip*, vol. 7, pp. 463–468, Apr. 2007.
[43] M. Kaya, S. Feingold, K. Hettiarachchi, A. P. Lee, and P. A. Dayton, "Acoustic responses of monodisperse lipid-encapsulated microbubble contrast agents produced by flow focusing," *Bubble Sci. Eng. Technol.*, vol. 2, pp. 33–40, May 2010.
[44] E. Talu, K. Hettiarachchi, R. L. Powell, A. P. Lee, P. A. Dayton, and M. L. Longo, "Maintaining monodispersity in a microbubble population formed by flow-focusing," *Langmuir*, vol. 24, pp. 1745–1759, Mar. 2008.
[45] E. Talu *et al.*, "Tailoring the size distribution of ultrasound contrast agents: Possible method for improving sensitivity in molecular imaging," *Molecular Imag.*, vol. 6, pp. 384–392, Nov. 2007.
[46] T. Segers and M. Versluis, "Acoustic bubble sorting for ultrasound contrast agent enrichment," *Lab Chip*, vol. 14, pp. 1705–1714, May 2014.
[47] T. Faez, I. Skachkov, M. Versluis, K. Kooiman, and N. de Jong, "*In vivo* characterization of ultrasound contrast agents: Microbubble spectroscopy in a chicken embryo," *Ultrasound Med. Biol.*, vol. 38, pp. 1608–1617, Sep. 2012.
[48] I. Skachkov, Y. Luan, A. F. W. V. D. Steen, N. D. Jong, and K. Kooiman, "Targeted microbubble mediated sonoporation of endothelial cells *in vivo*," *IEEE Trans. Ultrason., Ferroelectr., Freq. Control*, vol. 61, no. 10, pp. 1661–1667, Oct. 2014.
[49] T. J. A. Kokhuis *et al.*, "Secondary bjerknes forces deform targeted microbubbles," *Ultrasound Med. Biol.*, vol. 39, pp. 490–506, Mar. 2013.
[50] V. Garbin *et al.*, "Changes in microbubble dynamics near a boundary revealed by combined optical micromanipulation and high-speed imaging," *App. Phys. Lett.*, vol. 90, no. 11, p. 114103, 2007.

Tom van Rooij (S'15–M'16) was born in Eindhoven, The Netherlands, in 1987. He received the B.Sc. degree in biomedical engineering and the M.Sc. degree in medical engineering from the Eindhoven University of Technology, Eindhoven, in 2008 and 2012, respectively, and the Ph.D. degree from the Department of Biomedical Engineering, Thorax Center, Erasmus MC, Rotterdam, The Netherlands, in 2017. His thesis focused on ultrasound contrast agents for imaging and therapy through ultrahigh-speed optical imaging techniques, manufacturing and characterizing ultrasound contrast agents, and *in vitro* and *in vivo* ultrasound imaging and therapy.

He held a teaching position in 2012 at the Biomedical NMR Group, Department of Biomedical Engineering, Eindhoven University of Technology.

Inés Beekers (S'16) received the M.Sc. degree in applied physics specializing in medical imaging and acoustical wavefield modeling from the Delft University of Technology, Delft, The Netherlands, in 2015. She is currently pursuing the Ph.D. degree with the Department of Biomedical Engineering, Erasmus Medical Center, Rotterdam, The Netherlands, focusing on unraveling the mechanisms involved in ultrasound-enhanced drug delivery with contrast agents.

Kirby R. Lattwein received the M.Sc. degree in infection and immunity from the Erasmus Medical Center (Erasmus MC), Rotterdam, The Netherlands, in 2016. Her M.Sc. (*cum laude*) thesis focused on developing a novel therapy for infective endocarditis and sonobactericide, using ultrasound and ultrasound contrast agents against bacteria. She is currently pursuing the Ph.D. degree with the Department of Biomedical Engineering, Erasmus MC, focusing on the development of sonobactericide in both *in vitro* to *in vivo* settings. Her current research interests include innovative applications of ultrasound contrast agents.

During her thesis, she was a recipient of the Dutch Heart Foundation Student Scholarship, which allowed her to spend four months at Prof. C. K. Holland's Ultrasound Image Guided Therapeutics Lab, University of Cincinnati, Cinncinnati, OH, USA.

Antonius F. W. van der Steen (M'94–SM'03–F'13) received the M.Sc. degree in applied physics from the Delft University of Technology, Delft, The Netherlands, in 1989, and the Ph.D. degree in medical sciences from the University of Nijmegen, Nijmegen, The Netherlands, in 1994.

He was a Senior Scientist with the Laboratory for Experimental Echocardiography, Thoraxcenter, Erasmus University Medical Center (Erasmus MC), Rotterdam, The Netherlands, from 1994 to 1996, where he has been the Head of the Laboratory for Experimental Echocardiography since 1997. Since 2002, he has been a Full Professor and the Head of Biomedical Engineering with Erasmus MC. Since 2013, he has been a Full Professor of Applied Physics with the Delft University of Technology. Since 2013, he has also been an Honorary Visiting Professor with the Chinese Academy of Sciences, Shenzhen Institute of Advanced Technologies, Shenzhen, China. His current research interests include vulnerable plaque detection, intravascular imaging, biomechanics, ultrasound contrast agents, and transducer design for special applications.

Prof. van der Steen is a member of the Royal Dutch Academy of Science and The Netherlands Academy of Technology and Innovation (i.e., the Dutch Academy of Engineering). He is a Fellow of the European Society of Cardiology. He was a recipient of the 2000 NWO PIONIER Technical Sciences (Best Researcher of The Netherlands in technical science under 40) and the 2007 Simon Stevin Master (Best Researcher in translational research).

Nico de Jong (A'97–M'09) received the M.Sc. degree in physics specialized in the field of pattern recognition from Delft University of Technology, Delft, The Netherlands, in 1978, and the Ph.D. degree with a specialization in acoustic properties of ultrasound contrast agents in 1993 from the Department of Biomedical Engineering, Thorax Center, Erasmus MC, The Netherlands.

In 2003, he joined the University of Twente, Enschede, The Netherlands, as a part-time Professor. He currently teaches with Technical Universities and Erasmus MC. He has been a Promotor of 21 Ph.D. students and is currently co-supervising 11 Ph.D. students. Since 1980, he has been a Staff Member with the Thorax Center, Erasmus Medical Center (Erasmus MC), Rotterdam, The Netherlands. Since 2011, he has been a Professor of Molecular Ultrasonic Imaging and Therapy with Erasmus MC and the Delft University of Technology, and since 2015, he has been the part-time Head of the Department of Acoustical Waveform Imaging with the Delft University of Technology. Over the last 5 years, he has given more than 30 invited lectures and has given numerous scientific presentations for international industries. He has authored 260 peer-reviewed articles and has been a Principal Investigator (PI) and the Workpackage Leader of the European and Dutch projects. His H-factor is 46 (Web of science), and he has been acquired more than 6 M€ as a PI or a Co-PI since 2010.

Dr. Jong is the Organizer of the Annual European Symposium on Ultrasound Contrast Imaging, Rotterdam, which is attended by approximately 175 scientists from universities and industries all over the world. He is on the Safety Committee of the World Federation of Ultrasound in Medicine and Biology, and is an Associate Editor of *Ultrasound in Medicine and Biology*, and a Guest Editor of the special issues of different journals.

Klazina Kooiman (M'12) received the M.Sc. degree (*cum laude*) in bio-pharmaceutical sciences specializing in pharmaceutical technology from Leiden University, Leiden, The Netherlands, and the Ph.D. degree in ultrasound contrast agents for therapy from the Department of Biomedical Engineering, Thorax Center, Erasmus MC, The Netherlands, in 2011. She received the ICIN Fellowship in 2012, which enabled her to perform research for seven months from 2012 to 2013 at the laboratory of Prof. F. S. Villanueva, Center for Ultrasound Molecular Imaging and Therapy, University of Pittsburgh Medical Center, Pittsburgh, PA, USA. In 2014, she acquired the prestigious VENI grant from the Dutch Technology Foundation STW, which is part of the Netherlands Organization for Scientific Research and the Erasmus MC fellowship in 2015. She is currently an Assistant Professor and head of the Therapeutic Ultrasound Contrast Agent Group, Department of Biomedical Engineering, Thorax Centre, Erasmus MC, focusing on using ultrasound contrast agents for drug delivery and molecular imaging.

Dr. Kooiman was a recipient of the EFUSMB 2011 Young Investigator Award in Vienna. She is the Organizer of the Annual European Symposium on Ultrasound Contrast Imaging, Rotterdam, which is attended by approximately 175 scientists from universities and industries all over the world.